Numerical Simulation for the Determination of Hydraulic Fracture initiation and breakdown pressure using distinct element method

Hassan Fatahi, Md Mofazzal Hossain Seyed Hassan Fallahzadeh Masood Mostofi

Journal of Natural Gas Science and Engineering 33 (2016) 1219-1232

http://dx.doi.org/10.1016/j.jngse.2016.03.029

Abstract

Hydraulic fracturing technique has been widely used in many cases to enhance well production performance. In particular, this technology is proven to be the most viable technique for the oil and gas production from unconventional reservoirs. Accurate prediction of fracture initiation and breakdown pressure is vital for successful design of Hydraulic Fracturing operation. Methods of predicting these pressures include Analytical analysis, Field experiments, laboratory experiments and numerical simulations. Despite great achievements in the area of analytical analysis, they often failed to represent the true reservoir case, and consequently are found to be erroneous. Field tests such as mini-frac test are the best method for prediction of initiation and breakdown pressure. However, these tests are very limited due to their costs and are not very suitable for sensitivity analysis. Controlled laboratory tests seem to be the best option for predicting initiation and breakdown pressures. Test parameters such as fracturing fluid properties and principal stresses can be controlled with great precision to achieve accurate results. However, same as field tests, laboratory experiments are expensive. Core samples are limited and are expensive. Coring operation can take 4 to 5 days of rig time to take a 90 ft core. Geo-mechanical tests can take up to three days of a laboratory technician time per sample. Consequently, this will limit the number of tests to be done, and as a result it causes limitations on the conclusions that can be drawn from these tests. Simulation studies on the other hand do not have these limitations and can be used for as many times as desired to perform sensitivity analysis.

This paper presents a simulation model that is based on distinct element method. It is used to study the fracture initiation and breakdown pressure during hydraulic fracturing tests. The accuracy of the model was justified through comparison between laboratory experiments and numerical simulation. Four sandstone samples from two different sandstone types and a synthetic cement sample were used in the experimental studies. The tests were performed in True Tri-axial Stress Cell (TTC) with the capability to inject fluid into the samples. Simulation results demonstrate good agreement with experimental results. Fracture propagation path was found to be very similar. Fractures propagated in the direction of maximum horizontal stress.

1. Introduction

Hydraulic fracturing has been extensively used to increase production from low-permeable unconventional reservoirs (Tight gas, shale gas etc), enhance the productivity from a damaged well and mitigate sand production or water production issues. Execution of hydraulic fracturing treatment requires a proper understanding of the in-situ stress state, geo-mechanical properties of the formation as well as fracturing fluid dynamics. Accurate prediction of fracture initiation and break down pressure is one of the vital steps in designing a successful Hydraulic Fracturing operation. Different approaches

including analytical, numerical and experimental studies have been performed by many researchers to predict the fracture initiation and break down pressure. The classical analytical equation was derived by Hubbert and Willis [1] for a vertical wellbore in an infinite elastic medium based on the theory of elasticity. This equation has been further improved by Haimson and Fairhurst [2] to incorporate the effect of poro-elastisity. However, many experimental studies have demonstrated that these classical analytical equations do not match experimental results in most cases [3-8]. These experimental studies have shown that the breakdown pressure depends on fracturing fluid viscosity and compressibility, pressurization rate, deviatoric stress state, borehole size and presence of natural fractures that intersect the borehole. Therefore, alternative analytical equations have been developed and proposed by many researchers [3, 4, 7, 9-14]. Lakirouhani et al [13] presented the most comprehensive analytical study using a set of dimensionless parameters to simplify the equations. Yet, they assumed that the fracturing medium is elastic and impermeable. Since analytical solutions are derived based on certain assumptions such as homogenous elastic medium with no fluid leak off, they are subject to erroneous outcomes and contradictions with experimental and field operation results. Large scale field test is the best method of predicting accurate fracture break down pressure. However, improper knowledge of the in-situ stresses, rock properties and parameters associated with experimental test (e.g. flow rate, type, pressure rating, etc) may lead to misinterpretation of the test results. Since rock mechanical properties can accurately be determined in the laboratory and accurate stresses can be applied on the rock sample, probably the most accurate approach to predict the fracture break down pressure is the laboratory experimental tests. Yet, rock core samples are limited for test, and the test itself is involved with very laborious and time consuming exercises. Accordingly, it is not possible to run adequate tests for sensitivity analysis purposes. Numerical simulations can be developed to run as many sensitivity analyses as required. They can be more cost effective and require less time and resources.

Lhomme and de Pater [15] developed a method to study fracture initiation and propagation in an elastic homogenous permeable material. They assumed the fracture to be penny shaped. Finite difference method was then used to simulate their model in FLAC. They have validated the results by comparing them against laboratory results. Their laboratory tests were conducted on Colton Sandstone in a tri-axial stress cell. In this model, the fracture path was axi-symmetric and was known a-priori. Simulated initiation and breakdown pressures were consistently lower than experimental results. Pak and Chan [16] developed an implicit finite element numerical simulation. In this simulation, fracture is symmetric with respect to wellbore. They developed this simulation based on their thermo-hydro-mechanical analytical model. Model results were compared against Golder Associates [17] laboratory test results. These laboratory tests were conducted on oil sands in tri-axial stress cell. Although experimental and numerical breakdown pressures were close, the fracture propagation pattern was not same. Chudnovsky et al [18] developed a numerical method based on assumed penny-shaped hydraulic fracture growth. The model simulates the fracture as axi-symmetric. Model considered two cases of constant and variable fracture toughness with respect to hydraulic fracture radius size. Model results were compared to Wu et al [19] laboratory test results. Laboratory tests were conducted on edible-grade gelatine in a tri-axial stress cell. This material is brittle, elastic and impermeable. In these test, fracture initiation was observed to be same as fracture breakdown pressure. Comparison of the results showed that variable fracture toughness results are more realistic and closer to experimental outcome. Lecampion [20] performed analytical analysis to study fracture initiation, breakdown and propagation. He has shown that depending on parameters that affect hydraulic fracture; initiation and breakdown pressure can be different. Continuing the earlier numerical studies [13, 21, 22] and using his analytical

derivations, Lecampion built a numerical model based on Displacement Discontinuity Method. He discretised the continuity equation based on one-dimensional finite volume method. He assumed a constant fracture increment and based on this assumption calculated time step value. He then compared his numerical results to Zhao's [23] experimental result. Zhao conducted extensive experimental tests on Lac du Bonnet Granite. Hydraulic fracturing tests were performed in a tri-axial stress cell. Numerical-Experimental comparison was done for two cases of variable borehole size and variable pressurization rate. For both cases, numerical model and experiments showed the same trend. However numerical results were consistently higher than experimental results.

Numerical simulations developed so far show great achievements by researchers in this area. However, these models have one major limitation. These models are symmetric with respect to borehole. In few models the fracture path is known before simulation. Rigidity with respect to mesh is another limitation of these models. Once created, meshes cannot be changed easily and require further assumptions and simplifications. As a result, a more dynamic numerical simulation is required. Simulated fracture should be free to choose its path as it propagates and there should be no constraint on the path such as symmetry with respect to borehole. A mesh free simulation is also very desirable. The DEM numerical simulation that is used in this paper is not based on analytical derivations for fracture initiation and propagation, and therefore does not inherit the errors hidden in the analytical equations. Model is dynamic and fracture path is not constrained. Also the model doesn't require meshing, as it is comprised of discretised particles that are free to move with respect to each other. The simulation model is used to study the fracture initiation and breakdown pressures as well as fracture propagation path. In this method, fluid can leak off into the surrounding medium and can also flow through the fracture and does not need an assumption about the pressure profile inside the fracture. For comparison and validation of simulated results, five scaled hydraulic fracturing tests have been performed on three rock types in the laboratory. Dimensional analysis was carried out so that lab fracturing test could be considered as a proper representative of field scale fracturing treatment [24]. The model can very well replicate laboratory testing condition. Besides is does not face the obstacles present in laboratory testing, such as core availability or expensive sample preparation and test performance. It therefore, allows superior sensitivity analysis that allows more conclusions to be drawn.

2. Simulation Model: Structure and Mechanics

Distinct element method (DEM) based computer simulator, PFC2D, is used in this paper for simulation purposes. DEM and PFC2D have been explained in detail in author's earlier paper [25]. Further details can be found in Itasca documentations [26]. To build the simulation medium such as rock samples, circular particles are placed next to each other and are connected together by a bond. This bond resembles the bonding between particles in the real samples. Simulated rock samples should exhibit same mechanical properties as real samples. To calibrate simulated samples mechanical properties, a series of uniaxial compressive strength and confined compressive tests were performed. Simulated samples have a height of 95.25 mm and a width of 38.1 mm. These are the standard dimensions that were used for real sample for testing their mechanical properties. In this simulation, minimum particle radius was chosen as 0.3 mm and the ratio of maximum to minimum particle radius was 1.66. Simulated samples have two sets of mechanical properties. One set belongs to particles and bonds between particles. This set is called micro-mechanical properties. The second set is the mechanical properties of the bulk of the sample which are called macro-mechanical properties. This is analogous to real rocks

that are composed of grains. For example, a sandstone rock is composed of sand grains that are connected together by cement. Sand grains and cements have different mechanical and physical properties than sandstone. Grains have a density of 2.65 g/cc while bulk density depends on porosity. To calibrate macro-mechanical properties of simulated samples, their micro-mechanical properties need to be adjusted. Table 1 shows micro-mechanical properties of particles and bonds between particles. Macro mechanical properties of the simulated rocks are presented in Table 2 and show close agreement with experimental results. Simulation uses a seed number to generate random particles. To assure the model results and to make sure that they are reproducible, few simulations were performed. For each simulation, the seed number was changed to generate simulated samples with different particle arrangements. Macro-mechanical properties of the samples generated based on different seed number were very close. Reported values in Table 2 are average of five simulation test results. Further information regarding matching the mechanical properties of the simulated rock against real values and using PFC can be found in references [26] and [27]. Test plugs in different direction and from different parts of real samples were chosen for mechanical testing. Test results showed that mechanical properties were same in all directions and in all parts of the samples. This ensured that samples were homogenous and isotropic.

Table 1: Micro-mechanical properties of the sample

Property	**Unit**	**Value**		
		Sandstone 1	Sandstone 2	Mortar
Particle Young's Modulus	GPa	11	5.5	18
Particle Friction Coefficient	---	0	0	0
Particle Normal to Shear stiffness ratio	---	1.5	1.5	0.9
Parallel bond Young's Modulus	GPa	11	5.5	18
Parallel bond Normal Strength	MPa	1000	800	1000
Parallel bond moment contribution factor	---	1	1	1
Parallel bond cohesion strength	MPa	51	30	60
Parallel bond friction angle	°	80	64	66
Parallel bond normal to shear stiffness ratio	---	1.5	1.5	0.9

Table 2: Mechanical properties of real and simulated samples

Sample Type, ID	UCS (MPa)	Young's Modulus E (GPa)	Poisson's Ratio	Cohesion (MPa)	Internal Friction coefficient (°)
Sandstone 1	41.37	14.71	0.31	6.73	54
Simulated Sandstone 1	39.88	14.31	0.31	7.5	54
Sandstone 2	42.60	73.50	0.33	9.90	40.28
Simulated Sandstone 2	40.76	72.91	0.31	10.0	39.6
Mortar	79.50	27.70	0.2	17.40	44.3
Simulated Mortar	79	27.6	0.2	17	46

3. Simulation Model: Fluid Flow

The stage after preparing samples with desired mechanical properties is to set their fluid flow properties. In this stage porosity and permeability of the simulated samples should be matched against the porosity and permeability of real samples. In laboratory, these two parameters were measured on cylindrical dry samples. Samples were placed in a Helium Poro/permeameter apparatus. The apparatus is capable of applying boundary pressure on the sample. Permeability was measured using pulse decay method that uses helium as the flowing fluid. Using different pressures, it then extrapolated gas permeability versus reciprocal of pressure to calculate liquid permeability. Porosity was measured by the apparatus using the Boyle's law. These parameters are reported in Table 4 for different samples. Figure 1 shows a simulated sample. Particles are shown in grey colour. Centre of these particles are connected together to form a closed polygon which is called "Domain". Area of each domain shows its volume as out of plane dimension is considered to be one. This volume is multiplied by the real sample porosity to account for porosity of the sample. Black circles show volume of domains between particles that was adjusted by taking into account the porosity of the sample. The larger the size of the black circle, the bigger the volume of its corresponding domain. Fluid is stored in these domains. Each domain is connected to its neighbouring domains by black lines. Figure 2 shows a set of particles that form two neighbouring domains. Fluid flows between domains through an imaginary parallelepiped, which is considered to be at the contact point between particles. In the right hand side, the parallelepiped shown is considered to have aperture of w and length of L_p. In this way the 2D limitation of the simulation can be coped to make it comparable with 3D real samples. By adjusting the aperture of the parallelepipeds, the permeability of the sample can be adjusted. This aperture is not fixed though and can increase or decrease as the particles move toward or away from each other. Fluid flow through this parallelepiped follows the Poiseuille's equation for flow through parallel plates. Fracture happens when the bond between the particles break and particles move away from each other. This causes the aperture of the parallelepiped to increase and results in higher fluid flow at the point of the fracture. Fluid flow in DEM based models is however, comprehensively studied and the details of this fluid flow model is presented in first part of this study in the author's paper "Fluid flow through porous media using distinct element based numerical method" [25]. The same model presented in previous study is considered in current study for the fluid flow through hydraulic fracture. For measuring and adjusting the permeability, a dry sample similar to the one shown in Figure 1 with zero fluid saturation was simulated. Simulation was set in a manner that fluid could not cross the top and bottom faces of the sample. Fluid can cross the left and right boundary in a drained manner. Pressure at left end of sample was raised to 5 MPa and was kept constant at this pressure. Pressure at the right hand side was kept at 0 MPa. Fluid flow was measured at each time step between the left and right ends of the sample. In the simulation it was assumed that fluid flowed into domains and displacing air out. The flow process was considered to be immiscible. To account for saturation changes, all domains are considered inactive initially. In the inactive state, domain can accept fluid from higher pressure domains but they don't transmit any of it onto the lower pressure domains. Once the fluid pressure in domains reaches a threshold value, the domain becomes active and its saturation is set to one on V/V scale. Fluid was chosen as Newtonian for the simulation process. Once fluid flow rate got the same value and become stabilised, Darcy equation was used to calculate the permeability.

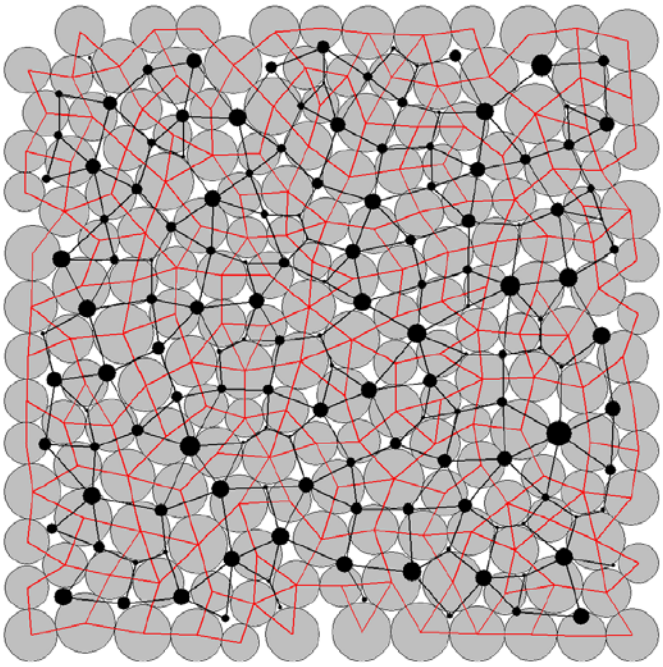

Figure 1: Collection of particles and domains. Grey circles show particles. Domains are polygons that are created by joining the centre of particles using red lines. Black circles show domain volumes that are equal to domain area times sample porosity. Out of plane dimension is equal to one. [25]

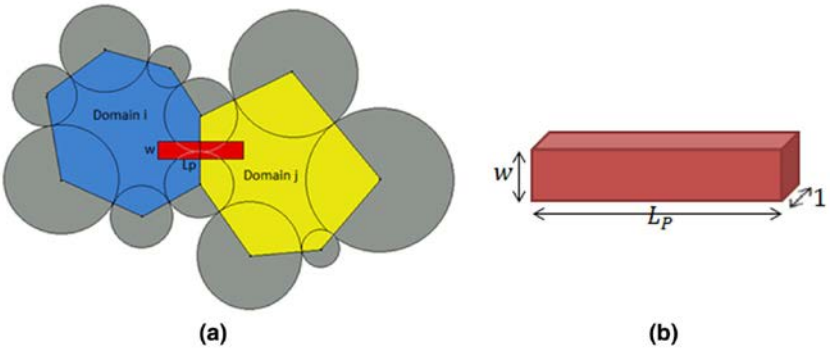

Figure 2: a- Two domains with a parallelepiped connecting them. b- Parallelepiped with aperture w and length L_p. Out of plane dimension is equal to one. [25]

4. Simulation of Hydraulic Fracturing

The aim of this study was to investigate the fracture initiation and breakdown pressure, fracture propagation with respect to the direction of minimum and maximum horizontal stresses and comparison of results against laboratory results. Sample that was calibrated for its mechanical and fluid flow properties from previous sections is used for this section. To simulate the borehole, particles in the centre of sample were removed. Sample was then subjected to minimum and maximum horizontal stresses. The next stage is to inject fluid into the borehole and monitor the wellbore pressure versus time. At the beginning of simulation, fluid volume into the borehole is zero. At each time-step, a constant volume of fluid is added to borehole to simulate constant injection fluid flow rate. Also at each time step, fluid leak off volume from borehole into the sample is calculated. Compressibility equations are used to calculate pressure change in each time step. At each time step, forces on particles because

of pressure and boundary condition stresses are calculated. These forces will move particles with respect to each other. As the pressure rises, borehole starts to expand. Particles at borehole wall start to move away from each other. This puts the particle bonds under tension or shear. Once the tensile or shear force on bonds exceeds the tensile or shear bond strength, these bonds will break. The first bond breakage between particles on the borehole wall corresponds to fracture initiation. Breakage of bonds one after each other corresponds to fracture propagation. At initial state, pressure inside borehole and sample is zero. Fluid pressure inside sample at top, bottom, left and right boundaries are kept constant at zero Pa. This is a drained test on a dry sample and fluid can move out of the sample at each boundary.

Simulation process is shown in Figure 3 for Sandstone 1.1. Figure 3a shows the sample that is enclosed by four frictionless plates. These plates introduce the maximum and minimum horizontal stresses on the sample. These plates only interact with sample particles. They don't interact with each other and can move freely with respect to each other. Plates are controlled by a servo control mechanism that moves them toward or away from sample to keep constant stresses on the sample. Figure 3b shows the sample with a small vertical crack. On the right hand side in this figure, the picture is zoomed-in to show a better view of the crack. For incorporation of crack, the bond between the particles is broken and replaced with smooth joint bond that has no strength. Information about bonds between the particles are elaborated in [26]. Figure 3c shows the start of fluid injection into the wellbore. The vertical axis shows the wellbore pressure in Pascals. The horizontal axis shows the time since the beginning of fluid injection. The blue circles show the normalized fluid pressure with biggest circle showing the highest pressure and smaller circles showing lower pressures. Figure 3d shows the fracture initiation with a closed up view at the right hand side. The fracture is shown as a red coloured line segment between two particles. The fracture initiates when the force on the particles pushes them away from each other and causes the bond between them to break. At this time the pressure starts to deviate from the linear trend. The reason for this deviation is that as the fracture initiates, the aperture of the parallelepiped between particles increases and fluid can easily flow through the parallelepiped away from wellbore and causes depressurization of the wellbore. Figure 3e shows the propagation of the fracture. It is seen from Figure 3e that even though the fracture has started, the pressure is still rising. This demonstrates that in this case, fracture breakdown and initiation pressures are different. Figure 3f shows the fracture breakdown pressure stage. This is the maximum pressure that wellbore can experience. It should be noted that this is the pressure in the wellbore and not inside the fracture. The pressure inside fracture is lower than wellbore pressure. Figure 3g shows the stages where fracture arrived at top boundary (left), bottom boundary (right) and a zoomed-in view of the fracture and pressure profile at the bottom. It can be seen from pressure profile that nearly one fourth of the fracture at each side away from wellbore has no fluid pressure. This is known as the fluid lag zone or the zone that the fracturing fluid has not penetrated yet.

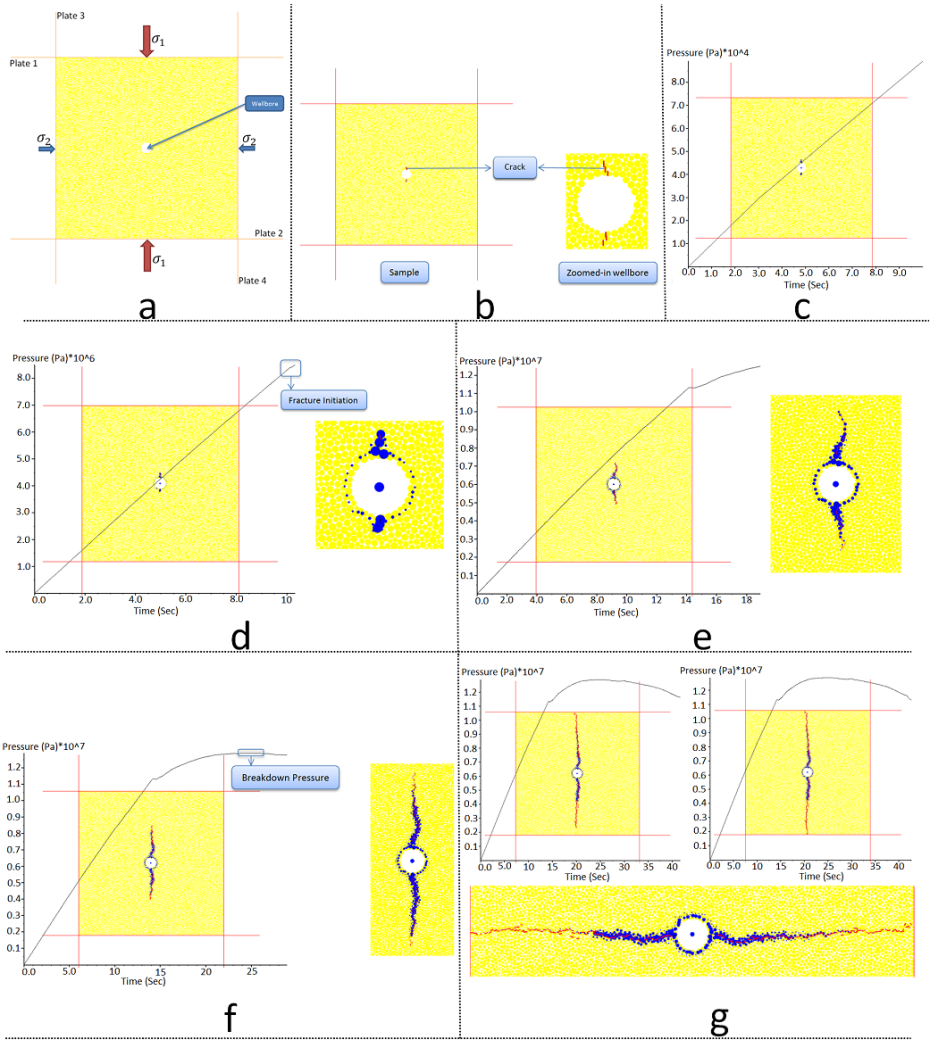

Figure 3: a-Sample with wellbore in the middle and four plates around it for stress installation. Horizontal maximum and minimum stresses are applied on the sample. b- Sample with vertical crack on left and zoomed in view at right. This represents initial crack in the direction of maximum horizontal stress in Sandstone 1.1. C- Beginning of fluid injection into the wellbore. Blue circles show normalized fluid pressure with biggest circle showing highest pressure. Vertical axis shows wellbore pressure and horizontal axis shows elapsed time since the beginning of fluid injection. Black diagonal line shows pressure versus time. d- Onset of fracture initiation. Red line shows created fracture. Pressure profile starts to deviate from linear trend by the creation of first fracture. e- Fracture propagation. Bonds between particles break one after each other. f- Fracture breakdown pressure is the maximum pressure that wellbore experience. g- Fracture arriving at top boundary (left), arriving at bottom boundary (right) and zoomed in view of fracture with pressure profile rotated 90^{o} clockwise.

Figure 4 shows extended flow period after fracture arrived at boundaries. At this stage the volume of the fluid injected into the wellbore is equal to the volume of fluid flow inside fracture and out of the sample. The rate of wellbore pressure drop was high at the beginning but it gradually decreased and becomes zero at steady state condition. At steady state condition, the wellbore pressure is equal to pressure required to keep the fracture open plus frictional pressure drop across the fracture. Because of the very low permeability of the sample and high fluid viscosity, the rate of leak off is very low but still considered to happen.

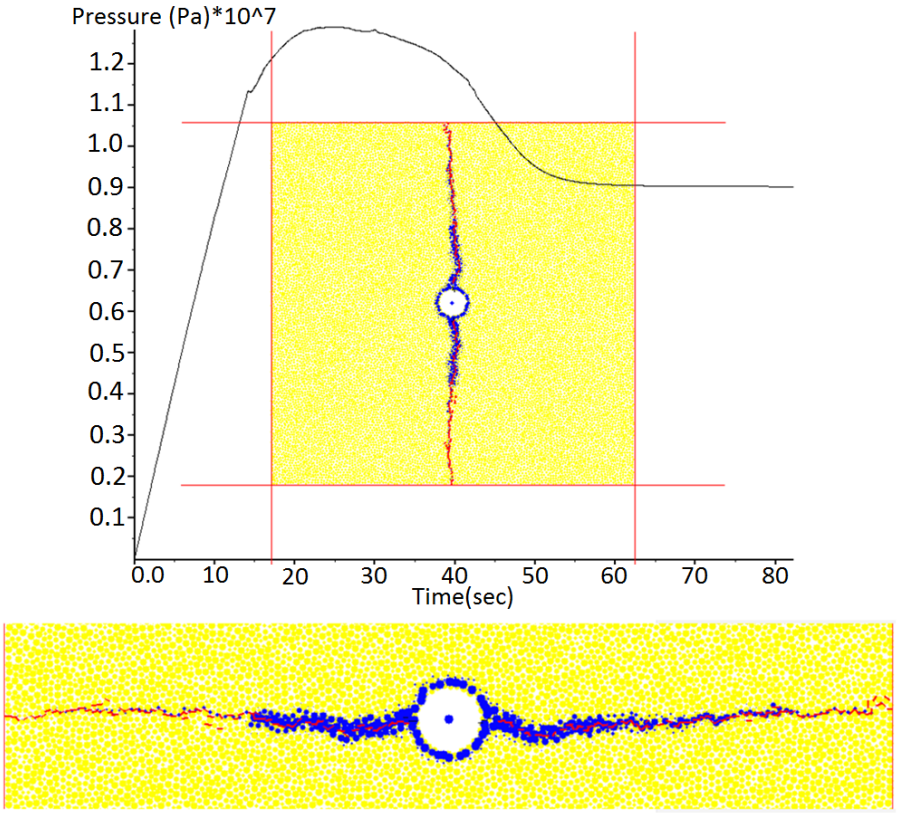

Figure 4: Stabilized flow through the fracture after fracture arrived at top and bottom boundaries. Pressure decline rate is high at the beginning when fracture arrived at boundaries. It gradually levelled off and got a constant value. The stabilized pressure value is equal to the pressure that is required to keep the fracture open plus the frictional pressure drop inside fracture. The bottom part of figure shows pressure profile inside fracture. Bottom picture is rotated 90° clockwise.

5. Laboratory Experiments

A rigorous experimental study was carried out in order to validate the simulation results. This study was carried out using True Tri-axial Stress Cell (TTSC). The experimental setup was developed based on the setup considered in previous study conducted by Sarmadivaleh [28, 29]. The detailed information about equipment, sample preparation, mechanical properties tests and test procedure can be found in this reference. A brief description of the equipment and test procedure is presented here.

Figure 5 shows a schematic view of the sample after preparation. A wellbore in the middle of one side of sample was drilled all the way to the opposite side. The top part of the hole was plugged and the middle section was left open with a vertical crack along wellbore axis. The bottom part was cased using a steel pipe.

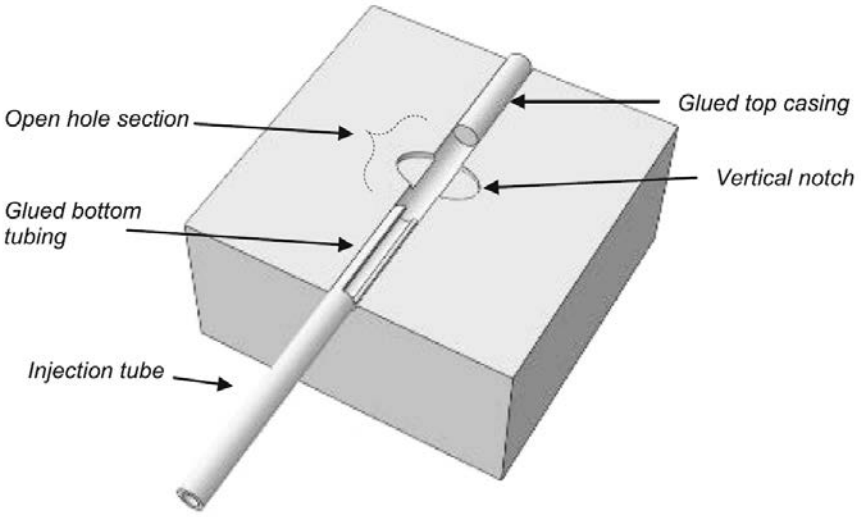

Figure 5: Schematic view of the sample showing the wellbore, top plug, bottom injection tubing and notch along the wellbore. [29]

Figure 6 shows a laboratory view of the TTSC equipment. The top part of the picture shows the whole apparatus. The bottom part of the picture shows the sample placement in the equipment. Sample is placed in the centre. Four spacers are placed between the sample and the loading plates. Loading plates are connected to loading rams. These rams will apply the horizontal stresses on the sample. Another spacer is placed on top of the sample. A hydraulic jack is then put on top of this spacer to apply the vertical stress on the sample. This configuration allows three independent stresses to be applied on the sample to simulate the realistic situation underground. The bottom part of the sample is connected to a pipe assembly. This pipe system is connected to a pump to inject fluid into the sample. Figure 7 shows the schematic view of the equipment configuration and sample placement. The top part of the figure shows the top view of the equipment. The bottom part shows the side view. The injection line has two pressure transducers close to the wellbore. There is a chock between these two transducers. These transducers are connected to a computer to record pressure versus time.

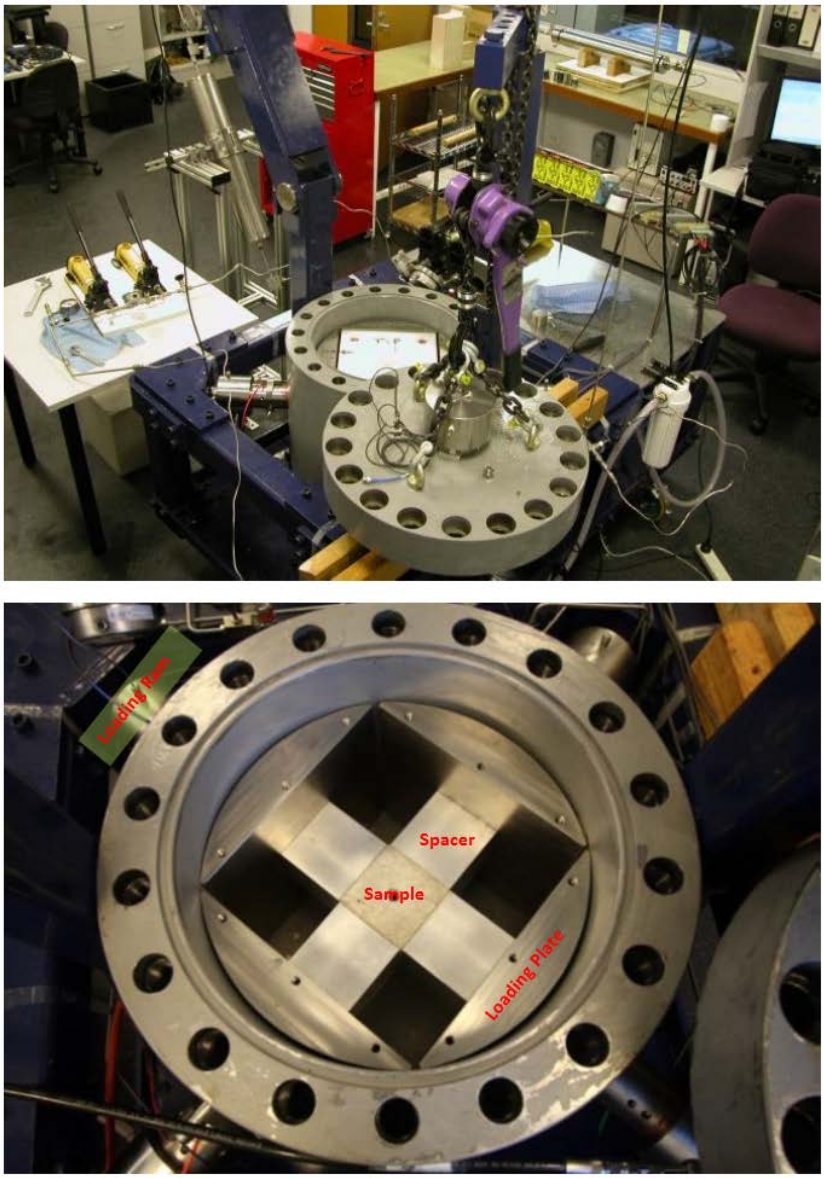

Figure 6: Laboratory picture of True Triaxial Stress Cell. Top view shows the whole apparatus. Bottom picture shows a 10 cm sample in the centre. Four spacers are placed between sample and loading plates. Loading plates are connected to loading rams. [28]

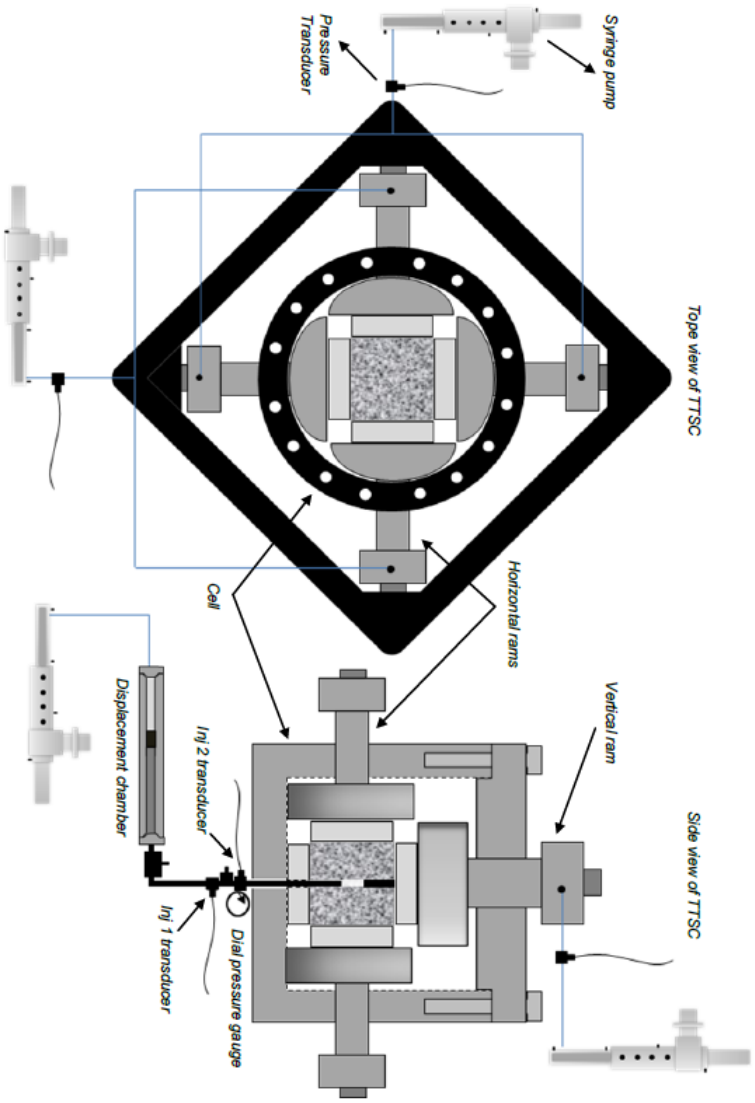

Figure 7: Schematic view of True Tri-axial Stress Cell. Top view of the apparatus is shown on the top. Side view of the apparatus is shown at the bottom. [28]

Figure 8 shows the pressure-time profile of laboratory hydraulic fracturing. There are two red and blue curves showing the pressure versus time. The blue curve shows the pressure recorded by pressure transducer represented as “Inj 2 transducer” in bottom part of Figure 7. The red curve shows the pressure recorded by the pressure transducer represented as “Inj 1 transducer”. As shown in Figure 8, these two curves fall on each other before fracture initiation. The reason is that, before fracture initiation, flow rate across chock is negligible. As a result, the pressure drop across chock is very small. During this stage the fluid is getting compressed in the system. Once the fracture initiates, extra volume in introduced to the wellbore that can receive fluid. This causes fluid flow across the chock and as a result a pressure drop across it. This causes the two red and blue curves to separate by the amount of pressure drop across the chock. To help identify initiation pressure with more accuracy, pressurization rate is also plotted. Before initiation, pressurization rate is constant. After initiation, the pressurization rate drops. The reason is that, fluid injection rate is constant, but system volume is increasing. Wellbore pressure can still increase to a maximum value that can be different from initiation pressure. This is

known as “Breakdown Pressure”. Weather breakdown pressure and initiation pressure are same or different will depend on test parameters. These parameters are flowrate, fluid viscosity, stress state and so on. The difference between the two has been analytically studied by Lakirouhani et al[13]. At this pressure, wellbore pressurization rate is zero. After breakdown pressure, wellbore pressure declines and pressurization rate gets a negative value. Wellbore pressure drops to a stabilized pressure. At this stage one or both wings of the fracture have arrived at boundary. Stabilized pressure is the pressure that is required to keep the fracture open plus pressure drop across the fracture because of fluid flow. At this stage, pressurization rate is zero.

In the numerical simulation, hydraulic fracture will always propagate in horizontal direction because of the 2D limitation of the software. The created fracture is parallel to the wellbore axis. To simulate this situation in the laboratory, vertical stress is greater than horizontal stresses. This forces the created fracture to be vertical and propagate in the horizontal direction.

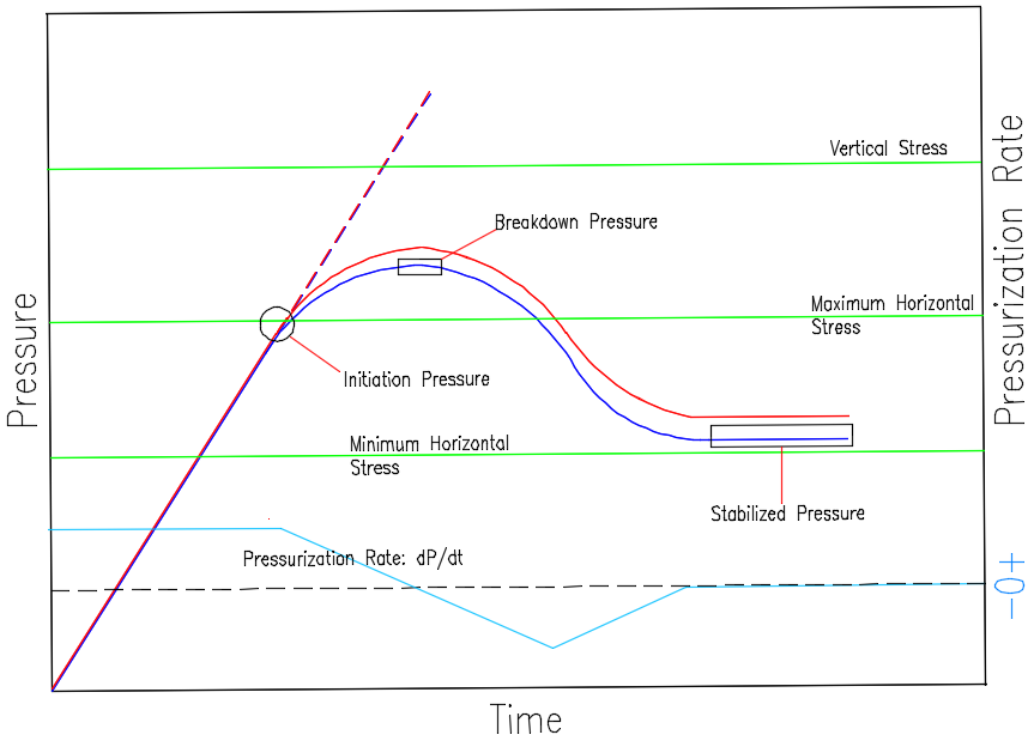

Figure 8: Hydraulic fracturing pressure profile. In laboratory two pressure gauges are installed near borehole with a chock between them. Blue curve shows the pressure from gauge closest to borehole. Red curve shows the pressure before chock. Before fracture initiation, both curves fall on each other. During this time, pressurization rate is constant. After initiation, pressurization rate drops and the two red and blue curves separate. Breakdown pressure is the maximum pressure that borehole experiences.

Cubical samples of side lengths specified in Table 3 were prepared. This table also shows wellbore diameter and wellbore section length. Table 4 shows fluid flow rate and viscosity as well as sample permeability and porosity. Lab experiments should properly represent field scale operations; therefore, dimensional analyses should be carried out and appropriate scaling laws should be followed. In order to develop the fracturing scaling laws, the fracturing mechanisms, which consist of different fracture propagation regime, must be analysed. It is the various fracturing mechanisms through which the

fracturing fluid energy is consumed. An unlimited number of fracturing mechanisms may exist in one specific fracturing process. However, one of these mechanisms would be the main energy dissipation source at a time, which is the main fracture propagation regime [30]. Considering the main propagation regime, fluid viscosity and injection rate, and fracture propagation time could be evaluated using the scaling laws. This requires knowledge of sample and borehole sizes, as well as its hydro-mechanical properties. Further description on the process of running scaled hydraulic fracturing test could be found in [31]. Table 5 shows principal stresses and notch direction for each of the samples.

Table 3: Sample and wellbore dimensions

Sample Type, ID	Sample Length (cm)	Sample Height (cm)	Sample Width (cm)	Wellbore Diameter (cm)	Wellbore Length (cm)
Sandstone 1.1	10	10	10	0.6	4
Sandstone 1.2	10	10	10	0.6	4
Sandstone 2.5	5	5	5	0.65	2
Sandstone 2.7	5	5	5	0.65	2
Mortar	10	10	10	0.7	4

Table 4: Flow rate, fluid viscosity, rock matrix permeability and rock porosity

Sample Type, ID	Flow Rate (cc/min)	Viscosity (cp)	Permeability (md)	Porosity (%)
Sandstone 1.1	0.1	100000	3	20
Sandstone 1.2	0.1	100000	3	20
Sandstone 2.5	0.1	100000	0.40	12
Sandstone 2.7	0.1	100000	0.40	12
Mortar	0.1	100000	0.02	15

Table 5: Principal Stresses and notch direction

Sample Type, ID	σ_V (MPa)	σ_H (MPa)	σ_h (MPa)	Notch status
Sandstone 1.1	17.93	13.79	6.89	In direction of σ_H
Sandstone 1.2	11.03	6.89	3.45	In direction of σ_h
Sandstone 2.5	10.34	0	0	No notch
Sandstone 2.7	10.34	6.89	3.45	In direction of σ_H
Mortar	20.68	13.79	6.89	In direction of σ_H

Figure 9 shows Sandstone 2.7 before and after hydraulic fracturing. Figure 9a shows the initial state of the sample. Figure 9b shows the sample with wellbore drilled through it. A saw was used to create the initial crack along the wellbore axis. Figure 9c shows the sample with injection pipe glued at the top. The bottom part was plugged by a piece of solid steel bar. Figure 9b&c show the state of stresses that were applied on the sample. Maximum horizontal stress was applied in the direction of initial crack.

Figure 9d,e&f show the sample after hydraulic fracturing. Hydraulic fracture initiated and propagated in the direction of maximum horizontal stress.

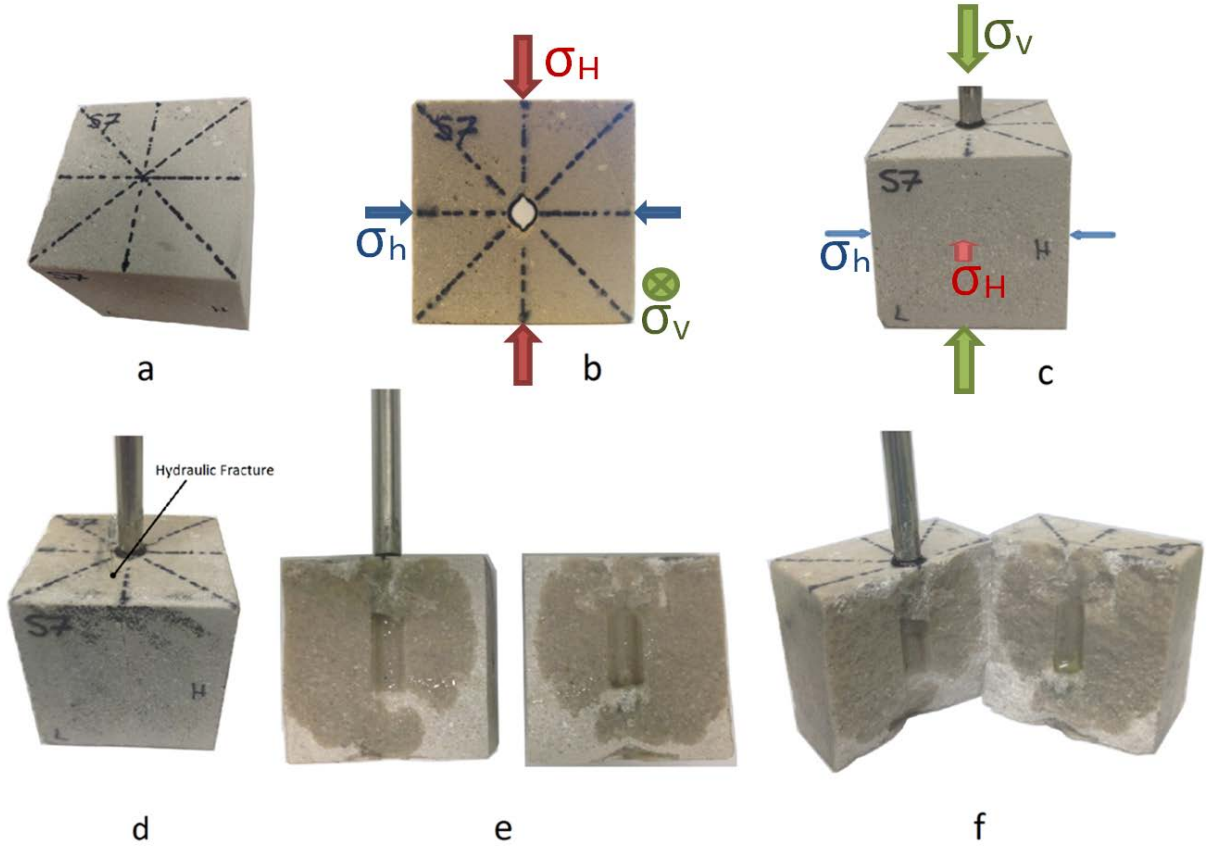

Figure 9: Sandstone 2.7. a) Prismatic sample, b) sample with hole drilled through and vertical notch, c) injection tubing glued to the sample, d, e, f) sample after hydraulic fracturing test. Figures b and c show the direction of principal stresses. Hydraulic fracture was created and propagated in the direction of maximum horizontal stress.

Figure 10 shows other samples tested. As it can be seen from Figure 10a, left wing of the fracture has deviated from the direction of maximum horizontal stress for Sandstone 1.1. This can be due to heterogeneous nature of the rock as real rock samples are not homogenous. The right wing aligned itself very well in the direction of maximum horizontal stress. Figure 10b shows Sandstone1.2. In this sample, the small initial crack is aligned in the direction of minimum horizontal stress whereas fracture initiated and propagated in the direction of maximum horizontal stress. As it can be seen the fracture is straight bi-wing with small tortuosity along the path. Figure 10c shows Sandstone2.5. This sample had no initial crack and no horizontal stress. Figure 10d shows a Synthetic Mortar sample. This sample has two slabs on each side that were cemented to the sample. The slabs were created similar to the main sample with same composition. The small crack was in the direction of maximum horizontal stress and a bi-wing fracture was created in the direction of initial small crack.

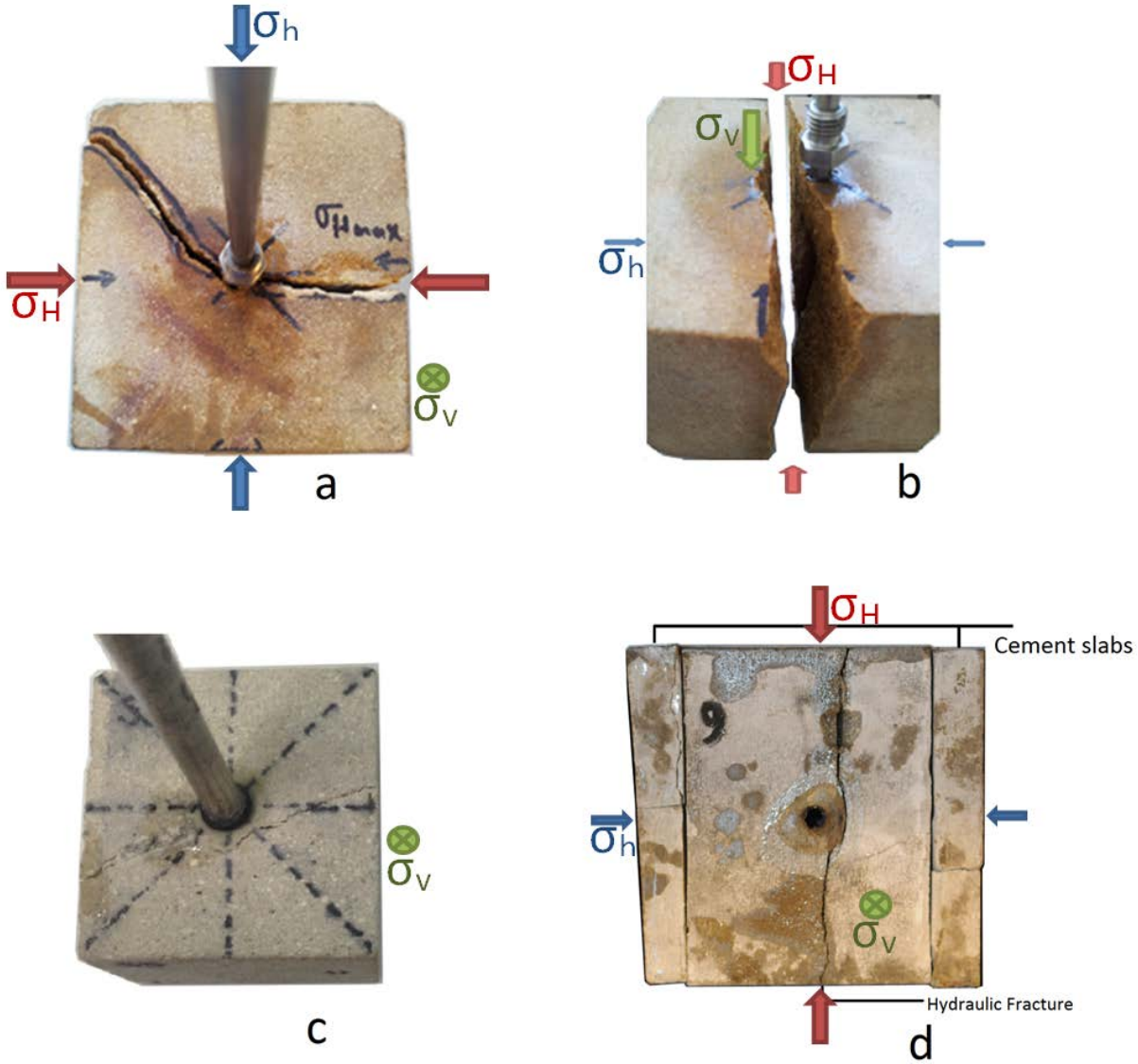

Figure 10: a- Sandstone 1.1 b- Sandstone 1.2 C- Sandstone 2.5 d- Mortar Sample. b and d show hydraulic fracture aligned itself very well in the direction of σH. For Sandstone 1.1 one wing of hydraulic fracture deviated away from σH direction. Sample 2.5 had no horizontal stresses.

6. Comparison between Numerical Simulation and Experimental Studies

This section provides a comparison between experimental and numerical simulation results. Simulated results are in close proximity to experimental results. These results are presented in Table 6. The percent difference between simulation and experimental results are calculated by subtracting simulation results from experimental results and dividing the difference times 100 by experimental results. Table 6 shows that differences are less than 10%. The smallest difference belongs to Mortar sample. The reason is that, synthetic samples are more homogenous than real rock samples. The fluctuation for the experimental breakdown pressure for same samples under same testing conditions are also observed in many studies [5, 6, 8, 9, 23, 32-39].

Figure 11 shows experimental and simulation pressure-time curves for Sandston 1.1 and 1.2. These rocks were tested at the early days that TTSC was installed. At the beginning, there was only one pressure transducer near borehole. This is the reason that there is only one curve showing borehole pressure. At that time, injection pump was manual and rate could not be controlled perfectly. Pressure fluctuations before breakdown pressure were a result of this issue. From these curves, initiation pressures could not be inferred. Only breakdown pressure which is the highest pressure on pressure-time curve can be picked. These issues were remedied after these tests. Better pressure-time curves were recorded later and are shown in Figure 12 and Figure 13. In Figure 11a&c, borehole pressure is shown in blue colour. Principal stresses are in green colour. Figure 11b&d show simulation pressure-time curve. In these figures, sample state after hydraulic fracturing is shown. Figure 12 shows the test results for Mortar sample. This sample has been experimentally studied by Sarmadivaleh [28]. As shown on the experimental plot, inferring initiation pressure is not straightforward. Author has picked up a different initiation pressure from what has been inferred in the reference. The author pick point is where the two dotted red lines cross each other. As shown on the plot, this is the time that the difference between Inj1 and Inj2 pressures started to increase. Figure 12 and Table 6 show that experimental and numerical initiation and breakdown pressures are very close to each other. Figure 13 shows test results for Sandstone 2.5 and 2.7. Figure 13a&c show Inj1 and Inj2 pressure transducer results in red and blue colours respectively. Principal stresses are shown in green colour. Pressurization rates are shown in cyan colour. The initiation point is where the two dotted lines cross each other. Figure 13c shows big fluctuations in pressurization rate after fracture initiation. Author thinks this might be because of some noise in pressure readings. It can also be because of some disturbance at pressure transducer and PC connection point. Figure 13b&d show simulation test results for sandstones 2.5 and 2.7 respectively. It also shows simulated sample state after fracturing test. Figure 13 shows close values between numerical simulation and experimental test results.

The major difference between the simulated and experimental pressure-time curves is the short time for simulated samples. Simulated test intervals are two orders of magnitude lower than experimental test interval times. For the real samples the injection system consists of the volume of oil in the injection pump and pipes, the volume of fracturing fluid in the fracturing fluid reservoir and pipes as well as the volume of wellbore. Volume of wellbore is observed to be very small as compared to volume of the rest of system. As the pressure builds up in the system, the oil and fracturing fluid will compress. Meanwhile the injection system that consists of pump, pipes and fracturing fluid reservoir will expand. This compression and expansion causes extra volume of fluid to be stored into the system. Once the fracture starts and reaches the boundary, it takes a long time for the whole system to depressurize. On the other hand, in simulation, the injection system only considers the volume of wellbore. So the volume of the fluid that is stored in the injection system will be very small and will take only few seconds to depressurize. In this paper, the focus was more on the fracture pattern and the initiation and breakdown pressures. To match the time of simulated hydraulic fracturing with experimental one, extra tests needs to be carried out to calculate the exact volume of oil and fracturing fluid in the system, the volume of pumps and pipes, and establish the relationship between the expansion of the volume of the injection system and injection pressure.

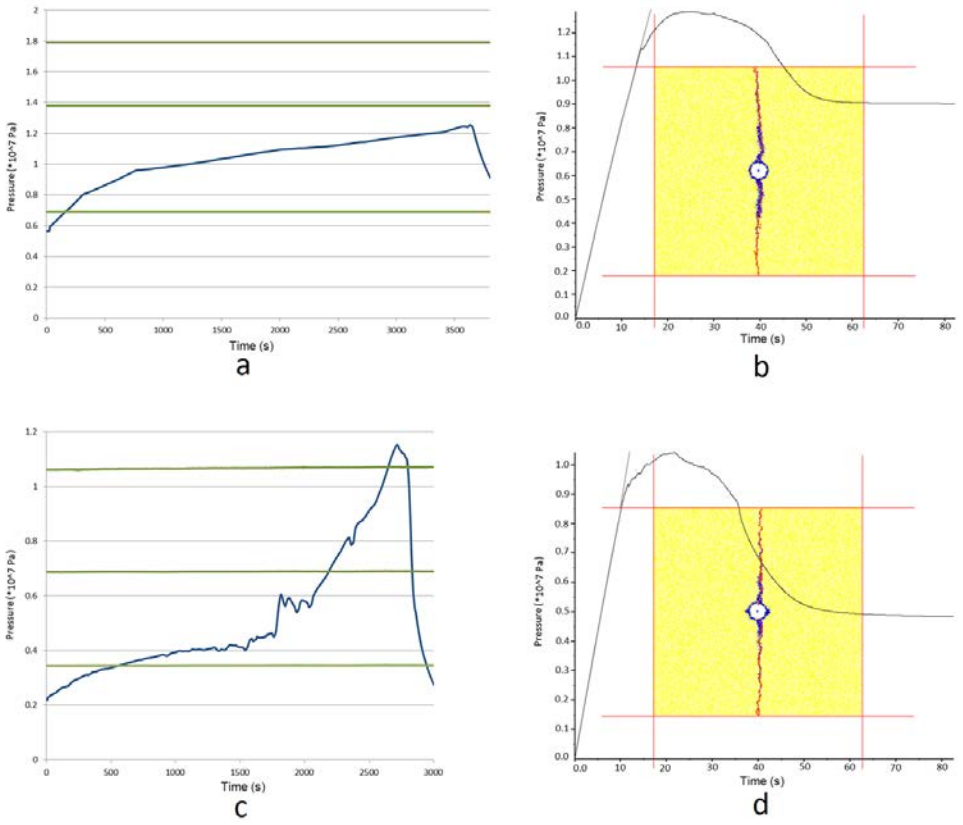

Figure 11: a- Experimental Pressure vs time for hydraulic fracturing Sandstone 1.1, b- Simulated Pressure vs time for hydraulic fracturing Sandstone 1.1, c- Experimental Pressure vs time for hydraulic fracturing Sandstone 1.2, d- Simulated Pressure vs time for hydraulic fracturing Sandstone 1.2. For each sample, simulated and experimental breakdown pressure values are very close. In the experimental plots green curves show principal stresses. Blue curve shows borehole pressure.

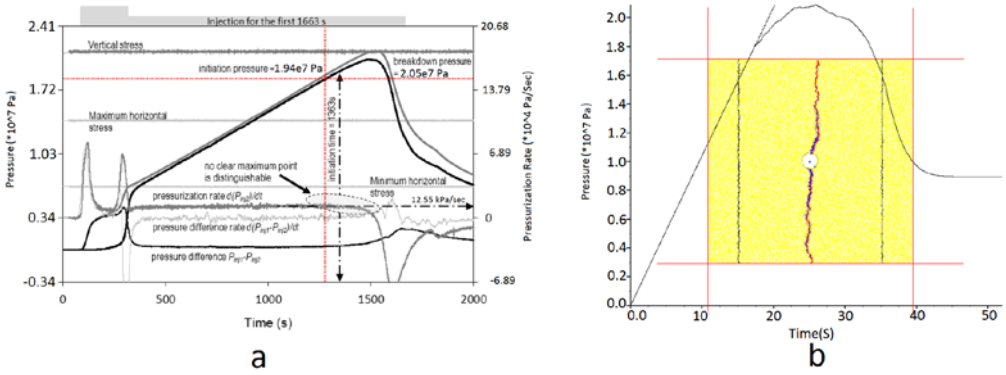

Figure 12: a- Experimental pressure vs time for hydraulic fracturing of Mortar sample. After Sarmadivaleh [28], b- Simulated pressure vs time for hydraulic fracturing of Mortar sample. Experimental and simulated initiation and breakdown pressures are very close.

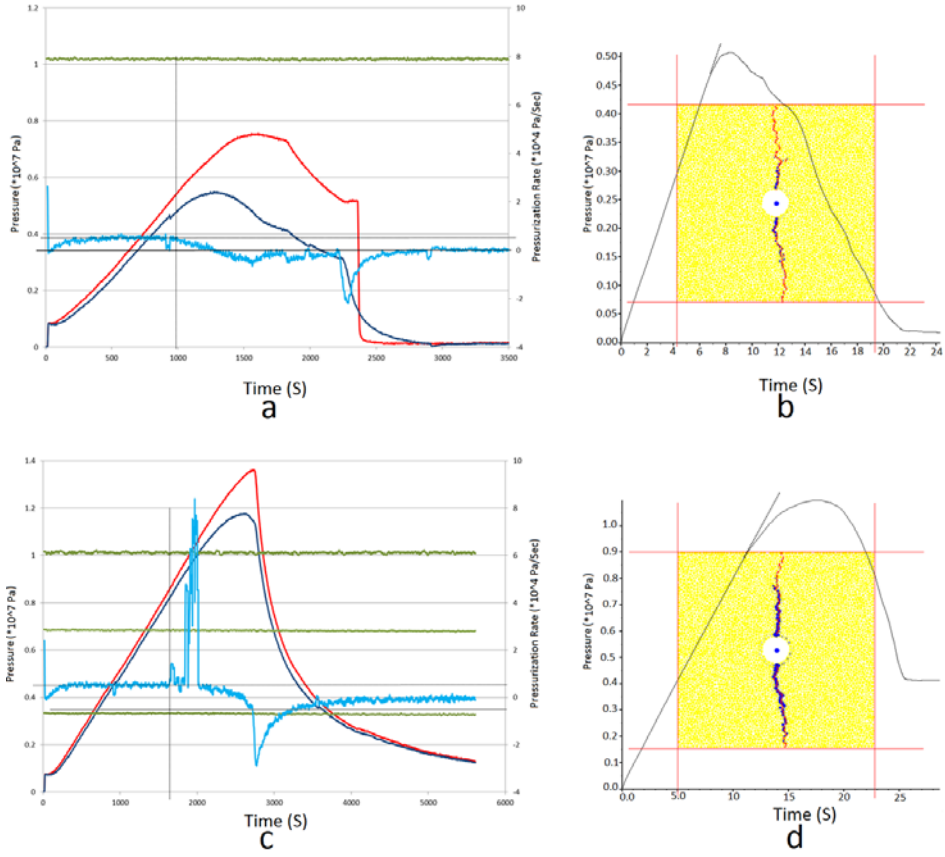

Figure 13: Pressure-time curve of hydraulic fracturing, a- Experimental pressure profile of Sandstone 2.5 b- Simulated pressure profile of Sandstone 2.5 c- a- Experimental pressure profile of Sandstone 2.7 d- Simulated pressure profile of Sandstone 2.7. In experimental plots, red and blue curve show pressure reading from Inj1 and Inj2 pressure transducers respectively. Green curves show principal stresses. Cyan curve shows pressurization rate calculated from Inj2 pressure transducer readings.

Table 6: Experimental versus Simulated initiation and breakdown pressures

Sample Type, ID	Simulated Initiation pressure (MPa)	Experimental Initiation Pressure (MPa)	% Difference	Simulated Breakdown pressure (MPa)	Experimental Breakdown Pressure (MPa)	% Difference
Sandstone 1.1	11.30	Not recognisable	---	12.91	12.50	-3.28
Sandstone 1.2	8.70	Not recognisable	---	10.44	11.51	9.30
Sandstone 2.5	4.54	4.66	2.58	5.09	5.48	7.12
Sandstone 2.7	8.90	8.1	-9.88	11.03	11.79	6.45
Mortar	18.0	18.3	1.64	20.91	20.55	1.75

7. Conclusion

This paper presented a simulation model that was developed using distinct element method (DEM). The model was used to study the fracture initiation and breakdown pressure during hydraulic fracturing tests. It also studied propagation path of hydraulic fracture with respect to principal stresses. The accuracy of the model was justified by comparing simulation results against experimental results. This model can be used for further sensitivity analysis to investigate many issues associated with hydraulic fracturing mechanism, and its initiation and propagation path behaviour for tight and heterogeneous reservoirs. The model has the ability to overcome some of the limitations prevail in existing analytical models, such as zero leak off or ambiguity about pressure profile inside fracture. However, the conclusions of current study are summarized below:

- The initiation and breakdown pressure are not necessarily same. Once initiation occurs, the pressure can still increase to reach the breakdown pressure. In other words, the fracture break down pressure is generally higher in some extent than the fracture initiation pressure.
- Initiation pressure can be inferred from the plot of pressure-time and pressurization rate-time plots.
- Once initiation occurs, pressure-time plot deviates from linear trend. Pressurization rate decreases after initiation time.
- Breakdown pressure is the maximum pressure on pressure-time plot.
- Pressurization rate at breakdown time is zero.
- Fracture propagates predominantly in the direction of maximum horizontal in-situ stress provided vertical stress is the maximum principal stress.

The 2D analysis is the limitation of this model. Future works can be done to develop a 3D model to overcome this limitation.

References

[1] M.K. Hubbert, D.G. Willis, Mechanics Of Hydraulic Fracturing, in, Society of Petroleum Engineers, 1957.
[2] B. Haimson, C. Fairhurst, Initiation and Extension of Hydraulic Fractures in Rocks, (1967).
[3] A.S. Abou-Sayed, C.E. Brechtel, R.J. Clifton, In situ stress determination by hydrofracturing: A fracture mechanics approach, Journal of Geophysical Research: Solid Earth, 83 (1978) 2851-2862.
[4] A.A. Daneshy, Hydraulic Fracture Propagation in Layered Formations, (1978).
[5] B.C. Haimson, Z. Zhao, Effect of Borehole Size And Pressurization Rate On Hydraulic Fracturing Breakdown Pressure, in, American Rock Mechanics Association, 1991.
[6] G.H. Boyce, T.W. Doe, E. Majer, Laboratory Hydraulic Fracturing Stress Heasurehents In Salt, in, American Rock Mechanics Association, 1984.
[7] W.L. Medlin, L. Masse, Laboratory Investigation of Fracture Initiation Pressure and Orientation, (1979).

[8] Z. Zhao, H. Kim, B. Haimson, Hydraulic Fracturing Initiation In Granite, in, American Rock Mechanics Association, 1996.
[9] F. Rummel, Fracture mechanics approach to hydraulic fracturing stress measurements, in: Fracture mechanics of rock, Academic Press London, 1987, pp. 217-239.
[10] E.E. Detournay, A.E. Cheng, Influence of pressurization rate on the magnitude of the breakdown pressure, in, American Rock Mechanics Association, 1992.
[11] D. Garagash, E. Detournay, A Study of the Breakdown Process In Hydraulic Fracturing Tests Conducted In Impermeable Rocks, in, International Society for Rock Mechanics, 1996.
[12] E. Detournay, R. Carbonell, Fracture-Mechanics Analysis of the Breakdown Process in Minifracture or Leakoff Test, (1997).
[13] A. Lakirouhani, A. Bunger, E. Detournay, Modeling Initiation Of Hydraulic Fractures From A Wellbore, in, International Society for Rock Mechanics, 2008.
[14] X. Zhang, R.G. Jeffrey, A.P. Bunger, M. Thiercelin, Initiation And Growth of a Hydraulic Fracture From a Borehole Under Toughness- Or Viscosity- Dominated Conditions, in, American Rock Mechanics Association, 2010.
[15] T.P. Lhomme, C.J. de Pater, P.H. Helfferich, Experimental Study of Hydraulic Fracture Initiation in Colton Sandstone, in, Society of Petroleum Engineers, 2002.
[16] A. Pak, D.H. Chan, A Fully Implicit Single Phase T-H-M Fracture Model for Modelling Hydraulic Fracturing in Oil Sands, (2004).
[17] C.C.f. Mineral, E. Technology, I.O.R.C. Limited, S.C. Limited, J.C.O.S. Ltd, A.O.S. Technology, R. Authority, G.A. Ltd, Laboratory Study of Hydraulic Fracture Propagation in Oil Sands, Phase III: Final Report, 1994.
[18] A. Chudnovsky, F. Fan, Y. Shulkin, H. Zhang, J.W. Dudley, G.K. Wong, Hydraulic Fracture Simulation Revisited, in, American Rock Mechanics Association, 2008.
[19] H. Wu, E. Golovin, Y. Shulkin, A. Chudnovsky, J.W. Dudley, G.K. Wong, Observations of Hydraulic Fracture Initiation and Propagation in a Brittle Polymer, in, American Rock Mechanics Association, 2008.
[20] B. Lecampion, Hydraulic Fracture Initiation From an Open-hole: Wellbore Size, Pressurization Rate And Fluid-solid Coupling Effects, in, American Rock Mechanics Association, 2012.
[21] E. Gordeliy, E. Detournay, A fixed grid algorithm for simulating the propagation of a shallow hydraulic fracture with a fluid lag, International Journal for Numerical and Analytical Methods in Geomechanics, 35 (2011) 602-629.
[22] B. Lecampion, E. Detournay, An implicit algorithm for the propagation of a hydraulic fracture with a fluid lag, Computer Methods in Applied Mechanics and Engineering, 196 (2007) 4863-4880.
[23] Z. Zhao, Determination of Far-field Stresses by Hydraulic Fracturing in Lac Du Bonnet Granite and Indiana Limestone, University of Wisconsin--Madison, 1995.
[24] S.H. Fallahzadeh, V. Rasouli, M. Sarmadivaleh, An Investigation of Hydraulic Fracturing Initiation and Near-Wellbore Propagation from Perforated Boreholes in Tight Formations, Rock Mechanics and Rock Engineering, 48 (2014) 573-584.
[25] H. Fatahi, M.M. Hossain, Fluid flow through porous media using distinct element based numerical method, J Petrol Explor Prod Technol, (2015) 1-26.
[26] Itasca, Particle Flow Code in 2 Dimensions, Fourth ed., Itasca Consulting Group Inc. , 2008.
[27] H. Fatahi, Simulation of Shale Mechanical Properties in PFC2d and Calibration of Them Against Lab Results for Tensile, Uni-Axial and Confined Compression Tests, in: SPE Annual Technical Conference and Exhibition, 27-29 October, Amsterdam, The Netherlands, Society of Petroleum Engineers, 2014, pp. 12.
[28] M. Sarmadivaleh, Experimental and numerical study of interaction of a pre-existing natural interface and an induced hydraulic fracture, Curtin University., 2012.
[29] M. Sarmadivaleh, V. Rasouli, Test Design and Sample Preparation Procedure for Experimental Investigation of Hydraulic Fracturing Interaction Modes, Rock Mechanics and Rock Engineering, 48 (2014) 93-105.
[30] A.P. Bunger, Near-surface Hydraulic Fracture, University of Minnesota, 2005.

[31] S.H. Fallahzadeh, A. James Cornwell, V. Rasouli, M. Hossain, The Impacts of Fracturing Fluid Viscosity and Injection Rate on the Near Wellbore Hydraulic Fracture Propagation in Cased Perforated Wellbores, in, American Rock Mechanics Association, 2015.
[32] B. Haimson, C. Fairhurst, Hydraulic Fracturing in Porous-Permeable Materials, (1969).
[33] M. Zoback, F. Rummel, R. Jung, C. Raleigh, Laboratory hydraulic fracturing experiments in intact and pre-fractured rock, in: International Journal of Rock Mechanics and Mining Sciences & Geomechanics Abstracts, Elsevier, 1977, pp. 49-58.
[34] D.R. Schmitt, M.D. Zoback, Laboratory Tests of the Effects of Pore Pressure On Tensile Failure, in, International Society for Rock Mechanics, 1989.
[35] B.C. Haimson, X. Huang, Hydraulic Fracturing Breakdown Pressure And In Situ Stress At Great Depth, in, International Society for Rock Mechanics, 1989.
[36] C.D. Martin, The strength of massive Lac du Bonnet granite around underground openings, in, University of Manitoba Manitoba, 1993.
[37] T.P.Y. Lhomme, Initiation of hydraulic fractures in natural sandstones, TU Delft, Delft University of Technology, 2005.
[38] Q. Gan, J.S. Alpern, C. Marone, P. Connolly, D. Elsworth, Breakdown Pressures due to Infiltration and Exclusion in Finite Length Boreholes, in, American Rock Mechanics Association, 2013.
[39] S. Asadi, B. Bohloli, M.R. Malekijavan, Numerical Investigation of Fracture Initiation And Propagation of Hydraulic Fracturing Based On Fracture Mechanics, in, International Society for Rock Mechanics, 2012.